Rapid Communications

Observation of accelerating solitary wavepackets

Georgi Gary Rozenman,[1,2] Lev Shemer,[3] and Ady Arie[2]

[1]*Raymond and Beverly Sackler School of Physics & Astronomy, Faculty of Exact Sciences, Tel Aviv University, Tel Aviv 69978, Israel*
[2]*School of Electrical Engineering, Iby and Aladar Fleischman Faculty of Engineering, Tel Aviv University, Tel Aviv 69978, Israel*
[3]*School of Mechanical Engineering, Iby and Aladar Fleischman Faculty of Engineering, Tel Aviv University, Tel Aviv 69978, Israel*

(Received 3 October 2019; accepted 1 May 2020; published 20 May 2020)

We study theoretically and observe experimentally the evolution of solitary surface gravity water wavepackets propagating in homogeneous and time-dependent flow created by a computer-controlled water pump, resulting in an effective linear potential. Unlike a potential free soliton, in this case the wavepacket envelope accelerates, while its phase is proportional to the cubic power of the position in the water tank. For increased wave steepness, we observe the emergence of asymmetry in the envelope, and hence it no longer retains its soliton shape. Furthermore, we study a case of ballistic dynamics of solitary surface gravity water wavepackets with initial nonzero momentum and demonstrate that their trajectory is similar to that of a projectile pulled by gravity. Nevertheless, their envelope shape is preserved during propagation, and the envelope phase is identical to that measured without an initial momentum.

DOI: 10.1103/PhysRevE.101.050201

A soliton is a wavepacket that maintains its shape while propagating at a constant velocity [1]. The unique properties of this wavepacket originate from the cancellation of nonlinear and dispersive effects in the medium [2]. The soliton was first described in 1834 by Russell who observed a solitary wave in the Union Canal in Scotland [2–4]. In the last few decades, solitons were extensively studied both theoretically and experimentally in various systems [5–8]. Most works deal with solitons of fluid dynamics, plasma physics, nonlinear optics, and matter waves [9–21]. These solitons are obtained as solutions of the nonlinear Schrödinger equation (NLSE) [22–24] in which both amplitude and phase play crucial roles from a theoretical and experimental point of view [25,26].

For deep surface gravity water waves, the time derivative of the water velocity potential acts as an external potential on the wavepackets [27]. Hence, waves propagating in a quadratic time-dependent flow (constant acceleration) are analogous to those that measure wave dynamics in a linear potential. Most studies deal with solitons propagating freely at a constant group velocity. However, such solitons may propagate in an external linear potential [28]. In a medium with cubic Kerr-type nonlinearity, such solitons accelerate and are governed by the nonlinear Schrödinger equation with an additional term that can be solved analytically [29]. The envelope of such a soliton retains a hyperbolic-secant shape, but its mean location accelerates with time. Furthermore, its phase exhibits not only a linear position-dependent phase, associated with a momentum change, but also a position-independent part that scales with the third power of time [29,30]. Such accelerating solitons appear in optical fibers, electromagnetic waves propagating in a plasma, dense astrophysical magnetoplasmas, Josephson junctions, and in Bose-Einstein condensates [31–37].

Despite the wide interest over the last 40 years in solitons in a linear potential, in different branches of physics, as far as we know, there is no direct experimental observation of the amplitude and phase dynamics of these solitons. The measurement of the cubic phase may be challenging, since, for example, interferometric measurements of electric fields are insensitive to the global position-independent phase [32]. We note that the cubic phase is also present in other wavepackets propagating according to a linear Schrödinger equation [24,27,38,39].

Here, we study the spatial propagation dynamics of nonlinear surface gravity water waves in an effective linear potential, realized by a well-controlled time-dependent homogeneous water flow. In particular, we focus on the evolution of hyperbolic-secant pulses in this arrangement, which is the analytic solution in a Kerr nonlinear medium, to gain insight into the corresponding electromagnetic problem. We confirm the prediction that solitons preserve their envelope shape as they propagate along a parabolic trajectory in a linear potential. Furthermore, we study, both theoretically and experimentally, the propagation dynamics of ballistic solitons, created by an initial momentum kick. We measure both their phases and amplitudes as they propagate in an external potential, and demonstrate that although their envelope follows a different path in a space-time diagram, their overall and cubic phase terms surprisingly remain unaffected. We further extend the measurement to a strongly nonlinear regime, in which the envelope becomes asymmetric and it no longer retains the symmetric soliton shape.

The analysis is based on the modified Schrödinger equation with an external flow. It is important to mention that in nonlinear optics both focusing and defocusing third-order nonlinearity is possible [40], whereas for deep surface gravity water waves, only focusing nonlinearity exists. Following Refs. [29,41], the scaled spatial version of the modified Schrödinger equation for the normalized amplitude envelope $A \equiv A(\tau, \xi)$ in the *moving frame* with the group velocity c_g is given by

$$i\frac{\partial A}{\partial \xi} = \frac{\partial^2 A}{\partial \tau^2} + F\tau A + |A|^2 A. \tag{1}$$

The scaled dimensionless variables ξ and τ are related to the propagation coordinate x and the time t by $\xi \equiv \varepsilon^2 k_0 x$ and $\tau \equiv \varepsilon\omega_0(x/c_g - t)$. The carrier wave number k_0 and the angular carrier frequency ω_0 satisfy the deep-water dispersion relation $\omega_0^2 = k_0 g$, with g being the gravitational acceleration; the group velocity $c_g \equiv \omega_0/2k_0$. The parameter $\varepsilon \equiv k_0 a_0$ characterizing the wave steepness is assumed to be small ($\varepsilon \ll 1$) in the linear regime and moderate $\varepsilon < 0.25$ in the nonlinear regime. The effective dimensionless force is related to physical units by $F \equiv -(\omega_0/\varepsilon^3 k_0^2)a_2$, where a_2 is the effective acceleration coefficient of the homogeneous flow, in units of $[\frac{s}{m^2}]$ and is obtained assuming that the wavepacket follows a parabolic trajectory $\langle t(x)\rangle = a_1 x + a_2 x^2$; $a_1 = c_g^{-1}$ is the inverted group velocity of the wavepacket.

The wavepacket envelope $A \equiv A(\tau, \xi)$ in the moving frame is governed by an equation that is similar to the one-dimensional temporal nonlinear Schrödinger equation of an electromagnetic wave in a linearly inhomogeneous plasma with cubic nonlinearity. However, for evolution in space rather than in time, the roles of time and space are interchanged [24,41,42].

The temporal surface elevation at the origin

$$\zeta(t, 0) \equiv a_0 \,\mathrm{sech}\left(\frac{t}{t_0}\right)\cos(\omega_0 t) \tag{2}$$

is prescribed by the wave maker at $x = 0$, where t_0 denotes the characteristic duration and a_0 is the maximum amplitude, and the dimensionless envelope A is related to physical units according to $A = \zeta/a_0$. The solitary wave solution of Eq. (1) has a normalized amplitude

$$|A^{(\mathrm{So})}(\tau, \xi)| = \mathrm{sech}[2\eta(\tau - F\xi^2)] \tag{3}$$

and the phase

$$\varphi_A^{(\mathrm{So})}(\tau, \xi) = -F\tau\xi + \frac{F^2}{3}\xi^3 + 4\eta^2\xi, \tag{4}$$

and the parameter η is the steepness-width ratio of the pulse and is given by $\eta = \frac{1}{2}(t_0\varepsilon\omega_0)^{-1}$. Equation (3) indicates that the soliton envelope maintains its shape, but accelerates owing to the linear potential. Equation (4) describes the evolution of the phase, with the first term representing linear with respect to the normalized time τ dependence with a slope that is proportional to ξ, i.e., this slope increases (also linearly) with the propagation coordinate; the second term in Eq. (4) is cubic in the spatial coordinate.

In order to measure the propagation dynamics of nonlinear surface gravity water wave pulses and the cubic phase, we conducted a series of experiments in a 5-m-long, 0.4-m-wide, and $h = 0.2$ m deep laboratory wave tank [27] with water waves moving in a time-dependent water flow (see Fig. 1). The velocity of the homogeneous flow increases linearly in time and is induced by a computer-controlled water pump. The experimental facility described, e.g., in Ref. [27] is capable of generating flow accelerations with F large enough to observe a parabolic trajectory in the space-time diagram. The wave maker is programed to excite wavepackets with a hyperbolic-secant envelope by a computer-controlled wedge that is partly immersed in the water and moves up and down. The carrier wave number $k_0 > 23\ \mathrm{m}^{-1}$ satisfies the deep-water condition $k_0 h > \pi$ [43]; the wave dissipation can be neglected. The pump and the wave maker as well as the specially designed inlet and outlet openings make it possible to generate a water flow with the required range of velocities and a high homogeneity. The temporal variation of the water velocity is monitored using a Pitot tube placed 2 cm beneath the surface. The realization of an effective linear potential for surface gravity water waves requires a linear increase of the water velocity with time. The velocity of the flow has been increased by 1.2 cm/s every second up to 12 cm/s for 10 s, yielding an acceleration of 1.2 cm/s^2. To avoid any effect of residual reflections from the beach located at the far end of the test section, measurements are performed at distances between 0.5 and 2.6 m from the wave maker. The instantaneous water surface elevations are measured by four wave capacitance-type wave gauges [44] mounted on a bar parallel to the tank side walls. The bar with the gauges is fixed to an instrument carriage that can be shifted along the tank. The water pump, the wave maker, and the data acquisition are synchronized using a single computer program. while the instantaneous surface elevation is measured by four capacitance-type wave gauges [44].

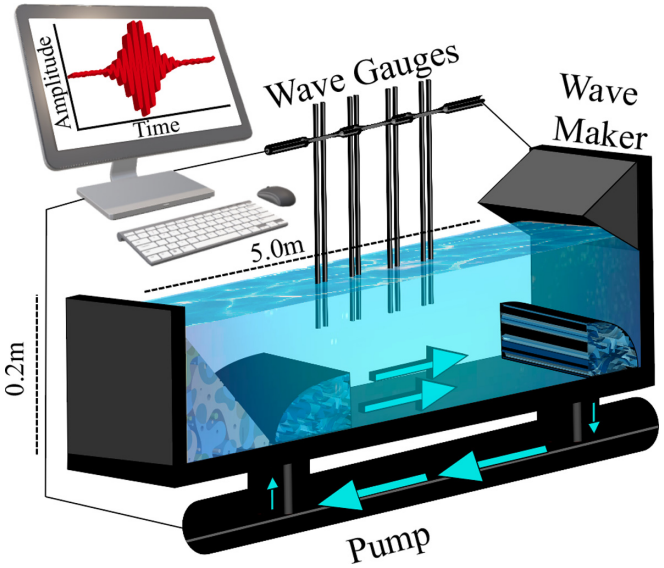

FIG. 1. Experimental setup for generating hyperbolic-secant surface gravity water wavepackets moving in a time-dependent homogeneous flow created by a water pump.

In order to extract the trajectory of the wavepacket in the laboratory frame, we calculate the mean temporal value, at a distance x from the inlet, defined as

$$\langle t(x)\rangle \equiv \frac{\int_{-\infty}^{+\infty} t|\zeta(t,x)|^2 dt}{\int_{-\infty}^{+\infty} |\zeta(t,x)|^2 dt}. \tag{5}$$

For each set of measurements a quadratic fit of $\langle t(x)\rangle$ is performed to extract the coefficients of the linear and quadratic terms a_1 and a_2, respectively. The envelope of the pulse is fitted to the hyperbolic-secant dependence

$$f = a_0^w \,\mathrm{sech}(t/t_w). \tag{6}$$

The varying with x width parameter t_w of the hyperbolic-secant pulse is obtained from the fit, as shown in Fig. 2. The expected parabolic dependence is fitted to the data

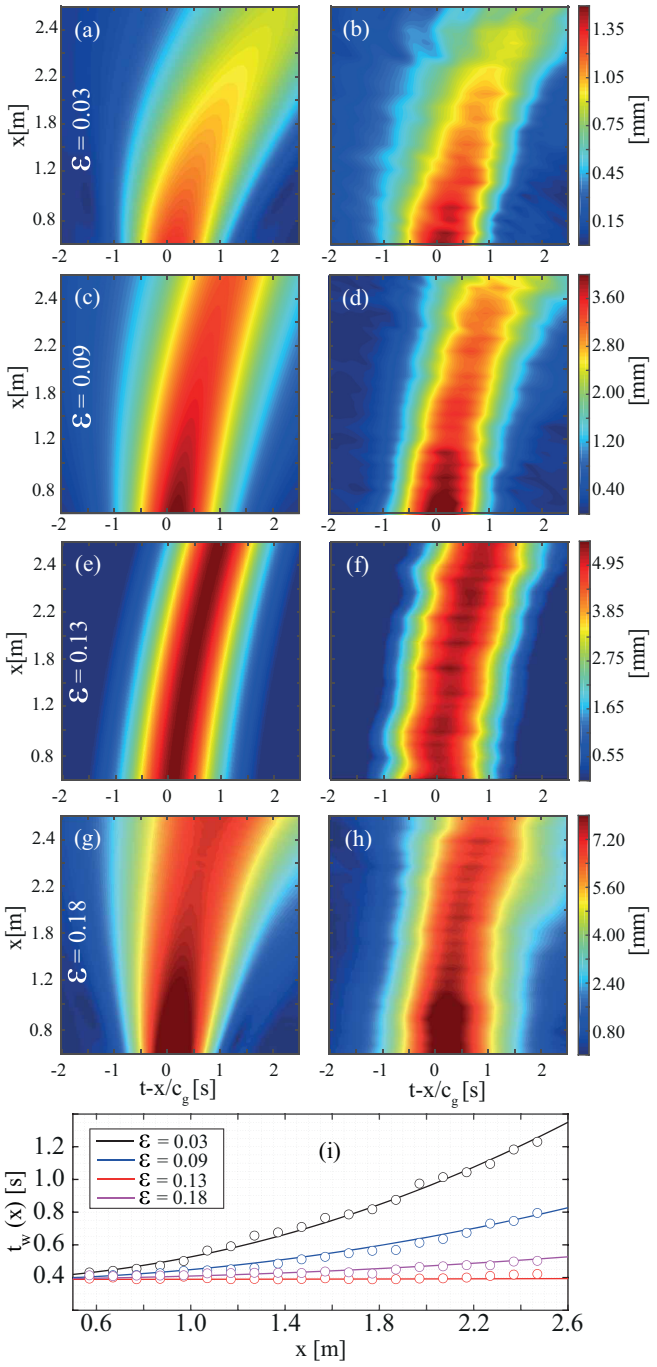

FIG. 2. Evolutions of hyperbolic-secant envelopes [right, obtained from the measurements by the Hilbert transform; left, simulated based on Eq. (1) for (a), (c), and (e) and based on (7) for (g), with $t_0 = 0.33$ s, $\eta = 0.3$ in a frame of reference at moving velocity c_g]. Simulations (left column) and measurements (right column) were performed at (a), (b) $a_0 = 1.5$ mm, $\varepsilon = 0.03$, (c), (d) $a_0 = 4$ mm, $\varepsilon = 0.09$, (e), (f) $a_0 = 5.50$ mm, $\varepsilon = 0.13$, and (g), (h) $a_0 = 8.0$ mm, $\varepsilon = 0.18$. (i) Experimental (point) and theoretical widths (solid lines), calculated using Eq. (6) for different values of steepness. While at low steepness ($\varepsilon = 0.03$) the width is dominated by dispersion, for the higher steepness ($\varepsilon = 0.13$), $t_w(x)$ exhibits soliton behavior, remaining constant throughout the entire measurement range. For the case of a highly nonlinear steepness ($\varepsilon = 0.18$), the width increases slowly with x.

presented in Figs. 2(b), 2(d) and 2(f). The velocity parameter $a_1 = 3.08$ s/m is in good agreement with $c_g^{-1} = 3.06$ s/m (calculated using the water wave dispersion relation), and $a_2 = 0.05$ s/m^2. This procedure yields $F = -0.69$.

The propagation dynamics of accelerating hyperbolic-secant pulses is investigated first for wavepackets with low steepness (initial amplitude $a_0 = 1.5$ mm, $\varepsilon = 0.03$). In this case, the Kerr nonlinearity is negligible, and the pulse spreads as it propagates owing to dispersion [see Figs. 2(a) and 2(b)]. However, as the steepness increases ($a_0 = 4$ mm, $\varepsilon = 0.09$), the enhanced nonlinearity reduces the spreading [see Figs. 2(c) and 2(d)]. The width of the pulses t_w is shown in Fig. 2(i), and the experimental data are presented in Figs. 2(b), 2(d) 2(f), and 2(h) and in Figs. 2(a), 2(c) and 2(d).

For even higher amplitudes, $a_0 = 5.5$ mm ($\varepsilon = 0.13$), the dispersion is compensated by the induced Kerr-type nonlinearity and the shape is preserved over a distance of 2.5 m [see Figs. 2(e) and 2(f)], thus providing clear experimental evidence of an accelerating solitary wavepacket. We further investigate higher amplitudes, up to $a_0 = 8.0$ mm ($\varepsilon = 0.18$), and observe that the wavepacket evolves asymmetrically and no longer preserves shape, in contrast to plasma waves which are governed by the NLSE that retain symmetry. Those strongly nonlinear wavepackets are modeled by the fourth-order modification of NLSE, also known as the Dysthe equation [24,41,42,45].

However, the original equation Dysthe has proposed does not include a term that describes an external homogeneous flow. Here, we propose a modification of the Dysthe equation, with an additional term $F\tau A$, where F is the dimensionless force presented above. The modified Dysthe equation in normalized form is

$$\frac{\partial A}{\partial \xi} + i\frac{\partial^2 A}{\partial \tau^2} + i|A|^2 A + 8\varepsilon|A|^2\frac{\partial A}{\partial \tau} + 2\varepsilon A^2\frac{\partial A^*}{\partial \tau} + F\tau A + 4i\varepsilon A\frac{\partial \Phi}{\partial \tau}_{Z=0} = 0, \quad 4\frac{\partial^2 \Phi}{\partial^2 \tau^2} + \frac{\partial^2 \Phi}{\partial^2 Z^2} = 0. \quad (7)$$

Here, Φ represents the envelope of the self-induced velocity potential, $\Phi = \frac{\phi}{\omega_0 a_0^2}$, and $Z = \varepsilon k_0 z$. The spatial coordinate z is a vertical coordinate pointed up vertically, $z = 0$, at the free surface.

The global phase change along the tank of accelerating hyperbolic-secant solitary wavepackets is presented in Fig. 3(a) in the laboratory frame with the same parameters as in Fig. 2(d); the black lines correspond to experimental data whereas the red lines correspond to Eq. (3).

The Hilbert transform [46] from the toolbox function "hilbert" [47] of *Matlab* is applied to extract the global phase change. The amplitude and phase induced during pulse propagation can be determined by creating a complex signal

$$z(t) \equiv u(t) + i \cdot H\{u(t)\}$$

from a real signal $u = u(t)$,

$$H\{u(t)\} \equiv \frac{1}{\pi}\int_{-\infty}^{\infty}\frac{u(s)}{t-s}ds.$$

Using the polar decomposition

$$z(t) = u(t) + iv(t) \equiv A(t)e^{i\varphi(t)}$$

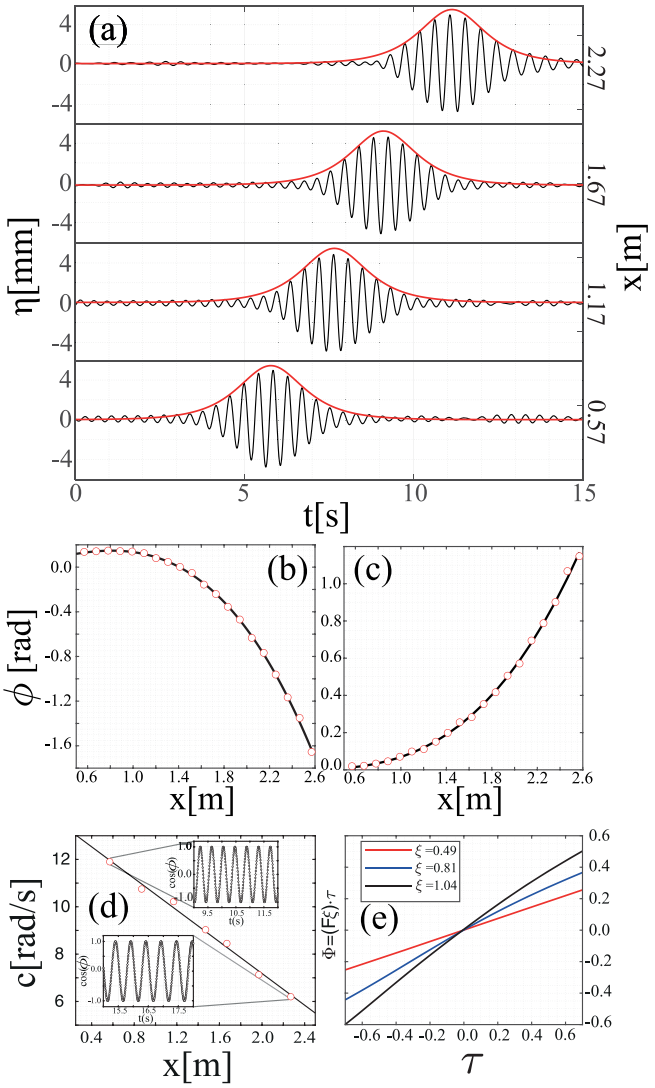

FIG. 3. Global phase change and accumulated cubic phase for accelerating solitary water wavepackets. (a) The observed surface elevation of wavepackets in different locations along the water tank; ζ^{So} (black line) and predicted by Eqs. (4) envelopes (red lines) for $k_0 = 23\ \mathrm{m}^{-1}$, $a_0 = 5.50$ mm ($\varepsilon = 0.13$), $c_g = 0.33$ m/s, and $t_0 = 0.33$ s. Quadratic fits were performed for 20 measuring points, determining $c_g = 1/a_1$ together with $F \equiv -0.69$. (b) The phase offset of the accelerating solitary water wavepacket at the maximum of the mean value of every elevation. (c) The cubic phase term, obtained by subtracting the linear terms from the global phase change shown in (b); for both (b) and (c) the red markers are the phase values given by the Hilbert transform from the surface elevations (after the removal of the carrier phase) and black solid lines are analytical results. (d) The slope c of the linear time-dependent function of the phase; each point is given by extracting $\cos(\phi)$ vs t. (e) The extracted linear phase term $\phi = F\xi\tau$ in the moving frame.

yields the instantaneous envelope amplitude

$$A(t) \equiv \sqrt{u^2(t) + v^2(t)},$$

and its instantaneous phase

$$\varphi(t) \equiv \arctan\left[\frac{v(t)}{u(t)}\right].$$

The remaining phase envelope (after removing the carrier part $k_0 x - \omega_0 t$) is plotted in Fig. 3(b); the red markers indicate the global phase change at 20 selected points along the water tank whereas the black lines correspond to Eq. (4). In order to extract the cubic term, we subtract the linear terms from the measured data, i.e., plot the term $\varphi_A^{(\mathrm{Cub})}(\tau,\xi) = \varphi_A^{(\mathrm{So})}(\tau,\xi) + F\tau\xi - 4\eta^2\xi = \frac{F^2}{3}\xi^3\varphi$. The cubic term is shown in Fig. 3(c), and the red markers indicate the global cubic phase change at 20 selected points along the water tank whereas the black lines correspond to $\varphi_A^{(\mathrm{Cub})}(\tau,\xi) = \frac{F^2}{3}\xi^3$.

We now show the linear part of the phase $\phi = F\xi\tau$ along the pulse at specific locations. This phase can be expressed as $\phi = \phi_0 + ct$, where ϕ_0 is the initial phase shift and c is the slope. The value of c can be obtained directly at different locations by fitting the experimental results of $\cos(\phi)$, as

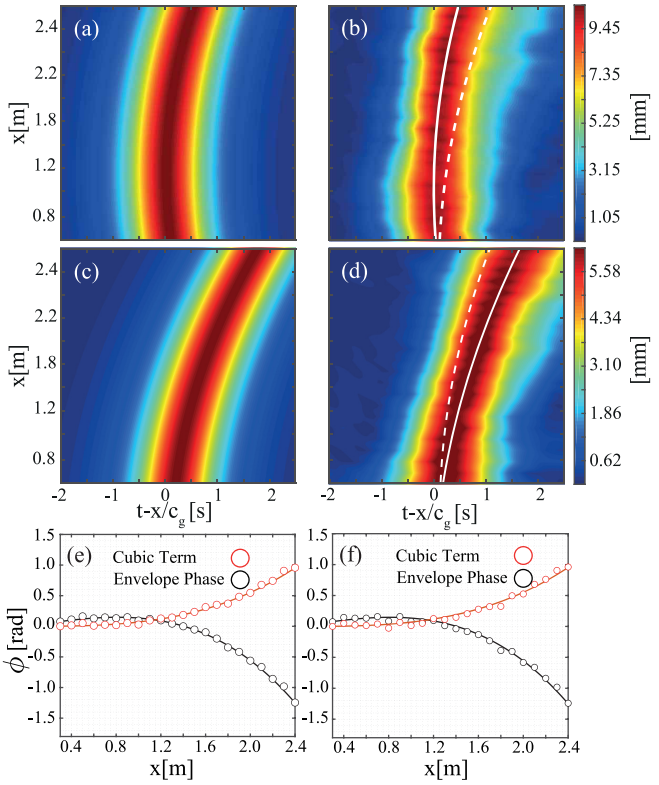

FIG. 4. Evolutions of hyperbolic-secant envelopes with an initial momentum kick [right, obtained from the measurements by the Hilbert transform; left, simulated based on Eqs. (18) with $t_0 = 0.66$ s], in a frame of reference at a moving velocity c_g (a), (c), and (e). Simulations (left column) and measurements (right column) for (a), (b) $a_0 = 10.5$ mm, $\varepsilon = 0.18$, $p_0 = -2$ rad/s, and (c), (d) $a_0 = 6.2$ mm, $\varepsilon = 0.18$, $p_0 = 2$ rad/s, and the effective force $F \equiv -0.69$. The global phase is measured by using the Hilbert transform for both (e) and (f). For both (e) and (f) the black markers are the measured global phase values (after the removal of the carrier phase) and black solid lines are analytical results given by Eq. (3). The red markers are the cubic phase terms, obtained by subtracting the linear terms from the global phase, i.e., an analytical subtraction of the linear terms $F\tau\xi - 4\eta^2\xi$, and red solid lines are analytical results given by $\varphi_A^{(\mathrm{Cub})}(\tau,\xi) = \frac{F^2}{3}\xi^3$. (e) presents the extracted phases from (b) and (f) corresponding to the measurements in (f), i.e., (e) corresponds to $p_0 = -2$ rad/s and (f) corresponds to $p_0 = 2$ rad/s.

shown in Fig. 2(d). The linear term of the envelope phase can be extracted explicitly via the Hilbert transform; the resulting slope of the phase corresponds to $F\xi$. This procedure provides direct observation of the increase of the linear phase term during propagation along the water tank, which appears only due to the acceleration of the solitary wavepacket, as shown in Fig. 3(e).

The existing setup is now used for studying solitary waves with a nonzero initial momentum. In this case, the soliton envelope of the temporal surface elevation is given by

$$\zeta^{(\mathrm{So/Ballistic})}(t,0) \equiv a_0 \,\mathrm{sech}\left(\frac{t}{t_0}\right)\cos(\omega_0 t)\exp(ip_0 t), \quad (8)$$

where p_0 is the analog of an initial momentum kick. We study the case of positive and negative initial momentum, i.e., $p_0 = \pm 2$ rad/s, resulting in a contribution of an initial velocity (in the moving frame) of $c_i = \pm 0.05$ m/s, where $c_i = g/2p_0$. In both cases, the trajectory is similar to that of a projectile pulled by gravity. Figure 4(b) clearly shows that for negative momentum $p_0 = -2$ rad/s at the beginning of the test section, the wavepacket propagates in the direction opposite to that of the acceleration, zero momentum is attained at approximately $x = 1.15$ m, followed by movement to the right. The white lines, given by $x = (a_2)(t - x/c_g)^2 + [g/(\omega_0 \pm 2p_0)](t - x/c_g)$, indicate the extracted using the Eq. (5) trajectory of the wavepacket in the moving frame; the white dashed lines shown for comparison are calculated for an accelerating wavepacket for $p_0 = 0$ rad/s. The difference between the solid and dashed lines shows that the ballistic wavepacket follows a different trajectory. This experiment was repeated for the case of positive momentum $p_0 = 2$ rad/s. Figures 4(c) and 4(d) show that the wavepacket propagates with a larger initial velocity. The solid white lines indicate that the trajectory of the wavepacket is indeed positively shifted compared to the nonballistic case, shown by the dashed white lines. The extracted phase values for the case of negative momentum, i.e., $p_0 = -2$ rad/s, are shown in Fig. 4(e), where the black markers show the global phase change (after the removal of the carrier phase) and the black solid lines are analytical results given by Eq. (4). In a manner identical to Fig. 3, we subtracted the linear terms and extract the cubic phase term, indicated by red markers; the analytical result $\varphi_A^{(\mathrm{Cub})}(\tau,\xi) = \frac{F^2}{3}\xi^3\varphi$ is given by solid red lines. The results shown in Figs. 4(e) and 4(f) are very similar to the case of the phase of nonballistic accelerating solitary wavepackets shown in Fig. 3. This observation indeed supports the theoretical prediction that the accumulated phase does not depend on the initial momentum and depends only on the distance of propagation ξ and on the effective force F. The global cubic phase is not limited to the hyperbolic-secant wavepackets studied here, but occurs for a wide variety of wavepackets moving in a linear potential in a nonlinear medium with a Kerr-type nonlinearity [31–35].

In conclusion, in a series of experiments, the propagation dynamics of solitary surface gravity deep-water wavepackets with and without initial momentum, which accelerate in a linear potential in a nonlinear medium, were observed. We have derived theoretically and measured successfully the acceleration of the solitary wavepacket envelope and the accumulated cubic phase of these wavepackets and have shown that despite having an initial momentum contribution (either positive or negative), the accumulated cubic phase is not affected. Moreover, by exciting wavepackets with a higher steepness in the water tank, higher-order nonlinear terms of the wave equation come into play, leading to asymmetric breaking of the soliton wavepacket solution. This procedure enables us to study the evolution of the amplitude and phase of wavepackets under the combined effects of asymmetry and linear potential, whereas in the past these effects were studied only for either asymmetry or a linear potential as mentioned in Refs. [28,48–52].

This work is supported by DIP, the German-Israeli Project Cooperation, the Israel Science Foundation (Grants No. 1415/17 and No. 306/15).

[1] L. Munteanu and S. Donescu, *Introduction to Soliton Theory: Applications to Mechanics* (Springer, New York, 2015).
[2] P. G. Drazin and R. S. Johnson, *Solitons: An Introduction*, 2nd ed., Cambridge Texts in Applied Mathematics (Cambridge University Press, Cambridge, UK, 1989).
[3] D. J. Korteweg and G. de Vries, London, Edinburgh Dublin Philos. Mag. J. Sci. **39**, 422 (1895).
[4] J. W. S. Rayleigh, London, Edinburgh Dublin Philos. Mag. J. Sci. **1**, 257 (1876).
[5] Y. S. Kivshar and G. Agrawal, *Optical Solitons* (Academic, London, 2003).
[6] L. D. Faddeev and L. Takhtajan, *Hamiltonian Methods in the Theory of Solitons* (Springer, New York, 2007).
[7] B. E. A. Saleh and M. C. Teich, in *Fundamentals of Photonics* (Wiley, New York, 1993).
[8] W. Liu, D. N. Neshev, I. V. Shadrivov, A. E. Miroshnichenko, and Y. S. Kivshar, Opt. Lett. **36**, 1164 (2011).
[9] Y. S. Kivshar and B. A. Malomed, Rev. Mod. Phys. **61**, 763 (1989).
[10] J. L. Bohn, B. D. Esry, and C. H. Greene, Phys. Rev. A **58**, 584 (1998).
[11] Z. Chen, J. Huang, J. Chai, X. Zhang, Y. Li, and B. A. Malomed, Phys. Rev. A **91**, 053821 (2015).
[12] D. N. Christodoulides, F. Lederer, and Y. Silberberg, Nature (London) **424**, 817 (2003).
[13] K. G. Makris, R. El-Ganainy, D. N. Christodoulides, and Z. H. Musslimani, Phys. Rev. Lett. **100**, 103904 (2008).
[14] H. Li, Z. Shi, X. Jiang, and X. Zhu, Opt. Lett. **36**, 3290 (2011).
[15] M. Q. Tran, Phys. Scr. **20**, 317 (1979).
[16] V. N. Serkin and A. Hasegawa, Phys. Rev. Lett. **85**, 4502 (2000).
[17] L. Shemer, E. Kit, and T. Miloh, Exp. Fluids **5**, 66 (1987).
[18] L. Shemer and E. Kit, Fluid Dyn. Res. **4**, 89 (1988).
[19] A. Chabchoub, B. Kibler, C. Finot, G. Millot, M. Onorato, J. Dudley, and A. V. Babanin, Ann. Phys. **361**, 490 (2015).
[20] L. Shemer, J. Fluid Mech. **217**, 143 (1990).
[21] K. E. Strecker, G. B. Partridge, A. G. Truscott, and R. G. Hulet, New J. Phys. **5**, 73 (2003).

[22] S. Fu, Y. Tsur, J. Zhou, L. Shemer, and A. Arie, Phys. Rev. Lett. **115**, 034501 (2015).
[23] S. Fu, Y. Tsur, J. Zhou, L. Shemer, and A. Arie, Phys. Rev. Lett. **115**, 254501 (2015).
[24] G. G. Rozenman, S. Fu, A. Arie, and L. Shemer, Fluids **4**, 96 (2019).
[25] N. K. Efremidis, V. Paltoglou, and W. von Klitzing, Phys. Rev. A **87**, 043637 (2013).
[26] A. E. Leanhardt, A. Gärlitz, A. P. Chikkatur, D. Kielpinski, Y. Shin, D. E. Pritchard, and W. Ketterle, Phys. Rev. Lett. **89**, 190403 (2002).
[27] G. G. Rozenman, M. Zimmermann, M. A. Efremov, W. P. Schleich, L. Shemer, and A. Arie, Phys. Rev. Lett. **122**, 124302 (2019).
[28] V. N. Serkin, A. Hasegawa, and T. L. Belyaeva, Phys. Rev. Lett. **98**, 074102 (2007).
[29] H. H. Chen and C. S. Liu, Phys. Rev. Lett. **37**, 11 (1976)
[30] X.-F. Pang and Y.-P. Feng, *Quantum Mechanics in Nonlinear Systems* (World Scientific, Singapore, 2005).
[31] A. Abdikian, WASET Int. J. Phys. Math. Sci. **11**, 7 (2017).
[32] K. E. Lonngren, Plasma Phys. **25**, 943 (1983).
[33] B. Guo, Z. Gan, L. Kong, and J. Zhang, *The Zakharov System and its Soliton Solutions* (Springer, Singapore, 2016).
[34] S. Aliand Ata-ur-Rahman, Phys. Plasmas **21**, 042116 (2014).
[35] A. Hasegawa, *Optical Solitons in Fibers* (Springer, New York, 1990).
[36] Q. Yang and J. Zhang, Opt. Commun. **258**, 35 (2006).
[37] A. L. Pankratov, A. V. Gordeeva, and L. S. Kuzmin, Phys. Rev. Lett. **109**, 087003 (2012).
[38] O. Amit, Y. Margalit, O. Dobkowski, Z. Zhou, Y. Japha, M. Zimmermann, M. A. Efremov, F. A. Narducci, E. M. Rasel, W. P. Schleich, and R. Folman, Phys. Rev. Lett. **123**, 083601 (2019).
[39] E. H. Kennard, Z. Phys. **44**, 326 (1927); J. Franklin Inst. **207**, 47 (1929).
[40] I. Kaminer, M. Segev, and D. N. Christodoulides, Phys. Rev. Lett. **106**, 213903 (2011).
[41] C. C. Mei, *The Applied Dynamics of Ocean Surface Waves* (Wiley-Interscience, Hoboken, NJ, 1983).
[42] L. Shemer and B. Dorfman, Nonlinear Process. Geophys. **15**, 931 (2008).
[43] L. Shemer, K. Goulitski, and E. Kit, Eur. J. Mech. B: Fluids **26**, 193 (2007).
[44] R. Chapman and F. M. Monaldo, J. Atmos. Ocean. Technol. **12**, 190 (1995).
[45] K. B. Dysthe, Proc. R. Soc. London, Ser. A **369**, 105 (1979).
[46] F. W. King, *Hilbert Transforms*, Vol. 1 (Cambridge University Press, Cambridge, UK, 2009).
[47] *Matlab* "Hilbert Transform" package, https://www.mathworks.com/help/signal/ug/hilbert-transform.html.
[48] S. Fu, Y. Tsur, J. Zhou, L. Shemer, and A. Arie, Phys. Rev. E **93**, 013127 (2016).
[49] M. Born and E. Wolf, *Principles of Optics* (Cambridge University Press, Cambridge, UK, 2002).
[50] M. V. Berry, R. G. Chambers, M. D. Large, C. Upstill, and J. C. Walmsley, Eur. J. Phys. **1**, 154 (1980).
[51] U. Bar-Ziv, A. Postan, and M. Segev, Phys. Rev. B **92**, 100301(R) (2015).
[52] G. A. Siviloglou, J. Broky, A. Dogariu, and D. N. Christodoulides, Phys. Rev. Lett. **99**, 213901 (2007).